Experimental Thermal and Fluid Science 109 (2019) 109873

Contents lists available at ScienceDirect

Experimental Thermal and Fluid Science

journal homepage: www.elsevier.com/locate/etfs

Jet dynamics during vaporization of water drops in hot oil films

Jeremy O. Marston*, Chao Li

Department of Chemical Engineering, Texas Tech University, Lubbock, TX 79409, United States

ARTICLE INFO

Keywords:
Liquid jets
Vaporization
Water peeling
surface tension

ABSTRACT

We experimentally investigate the vaporization of water droplets immersed in a hot oil film, with moderate temperaturedifferentials of 30–50 °C. In this regime, only a fraction of the water droplet vaporizes, but results in a symmetric vertical jet of oil. We provide detailed high-speed imaging of the physical process and quantitatively describe the vapor bubble growth, jet formation, jet speed and satellite droplets resulting from the jet break-up. The principal findings are that the jet speeds ($v_{jet} \sim O(1)$ m/s) are inversely correlated to the oil film thickness ($\delta \sim O(1)$ mm), whilst the surface tension-driven break-up results in primary satellite droplets whose normalized diameters also scale inversely with film thickness. Lastly, we provide observations of a water 'peeling' mechanism which occurs inside the vapor bubble, leading to a re-entrant jet that ultimately causes a secondary vaporization event.

1. Introduction

Liquid jets emanating from fixed-diameter orifices have been the subject of intense research for well over a century, dating back to pioneering works by Savart [32], Plateau [27] and Rayleigh [29], and for thorough reviews of the physics of this process, we refer the reader to the reviews by Lin and Reitz [20] and Eggers and Villermaux [12]. For recent practical applications, understanding jet dynamics has been important in processes such as ink-jet printing (e.g. [25,18]), pharmaceutical applications such as needle-free injection (e.g. [25]), water jet cutters, and prilling (e.g. [36]). In some cases, understanding and controlling the jet breakup to achieve a desired drop size distribution is key (e.g. [26,17]). In these applications, the driving mechanism for the jet is simply application of a pressure drop across an orifice to achieve a fixed flow rate. In contrast, jets may also result from flow-focusing due to rapid free surface disturbances, such as pressure impulse on a convex or concave meniscus (e.g. [2,34,33]), cavity collapse (e.g. [11,5,14,16]), hollow relaxation (e.g. [15]) droplet-wrapping (e.g. [22]) and droplet rebound from hydrophobic surfaces (e.g. [3]). Vertical jets from an initially quiescent film have also been reported from the rapid expansion of sub-surface laser-induced vapor cavities (e.g. [8,10,7,23]). This last mechanism is the closest to that observed in the present study, which pertains to jets created by water vaporization in hot oils.

Most humans have encountered water interacting with hot oils, typically when cooking. The phenomenon is particularly memorable as the result of hot fluid impingement onto one's skin, which can be quite painful. However, a slow-motion analysis of this event, permitted by high-speed videography, reveals a vastly rich dynamical process, as seen in Fig. 1(a). This violent release of small droplets is termed 'explosive vaporization'. This mechanism, whilst potentially hazardous due to propensity for fires [21], occurs only above a critical superheat temperature $\Delta T = T_o - T_{boil} > \Delta T^*$, where T_o is the oil temperature and T_{boil} is the boiling point of the liquid droplet, and will be dealt with in a subsequent publication. Here, however, we focus our attention on temperature differentials below this critical level, where we have discovered a more intricate vaporization regime that results in vertical liquid jets, as shown in Fig. 1(b).

The most relevant publications to date, which report observations of room-temperature droplets impacting onto hot oils are those of Manzello et al. [21], Lan et al. [19], and Alchalabi et al. [1], all of which report the explosive vaporization regime. In Table 1 and Fig. 2 we provide a comparison of the parameter ranges of those studies along with that of the present study. We note that the work of Frost [13] contains some of the earliest photographic evidence of explosive boiling, but this was for a completely immersed system for which the study parameters cannot be easily approximated. One interesting feature of the study by Manzello et al. [21] is that vapor explosions were observed for water with temperature differentials $\Delta T \approx 120$, but not for HFE-7100 ($T_{boil} = 61$ °C) when $\Delta T \gtrsim 120$. In contrast, the study of Alchalabi et al. [1] did report vapor explosions for a fluorinated liquid, PP1 ($T_{boil} = 57$) with $\Delta T \approx 100 - 200$ (see Table 2).

In the present work, the jetting regime is introduced and we seek to quantitatively describe the dynamics of the jet, such as jet diameter,

* Corresponding author.
E-mail address: jeremy.marston@ttu.edu (J.O. Marston).

https://doi.org/10.1016/j.expthermflusci.2019.109873
Received 1 March 2019; Received in revised form 28 June 2019; Accepted 9 July 2019
Available online 13 July 2019
0894-1777/

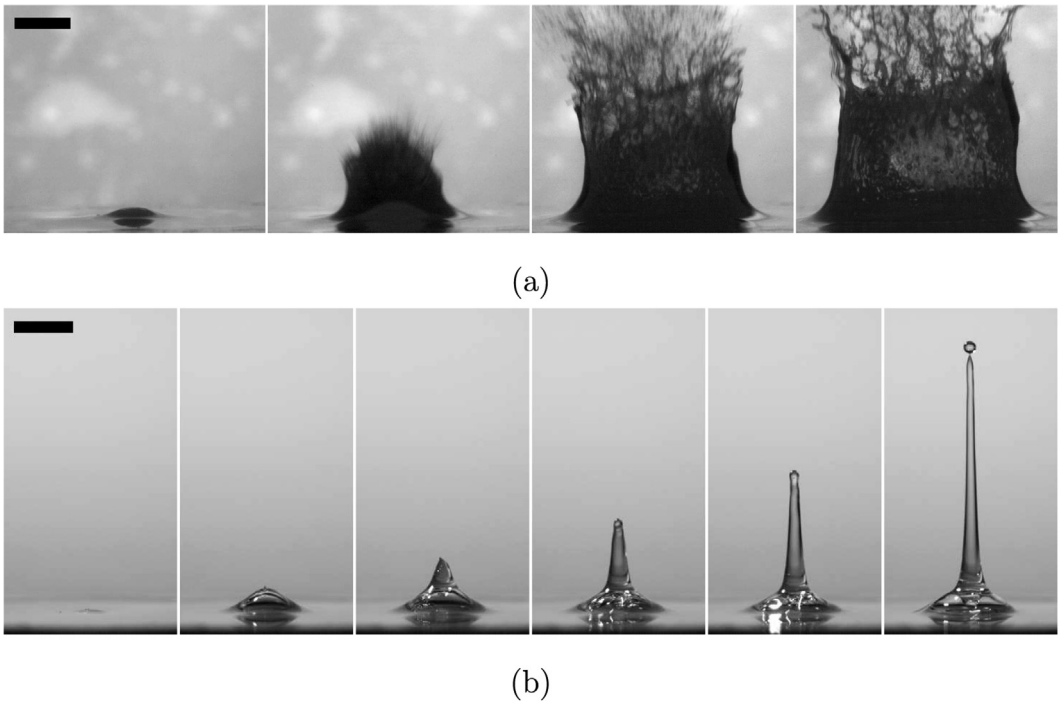

Fig. 1. (a) High-speed video sequence of an explosive vaporization event for a water droplet submerged in a 3 mm oil film with $T_o \approx 200$ °C. the scale bar is 5 mm and the time between frames is 0.75 ms. (b) High-speed video sequence of a partial vaporization event in a 3 mm oil film with $T_o \approx 150$ °C resulting in a vertical jet. The scale bar is 1 cm and the times are $t = 0$, 1, 3, 6, 10, and 22 ms.

Table 1
Summary of the key parameters used in the present study and those from Refs [1; 20; 21]. Note that the temperature differential is specified as $\Delta T = T_o - T_{boil}$, where T_{boil} is the boiling temperature of the liquid droplet.

Study	Ref.	Drop diameter	Pool depth	Temp. differential	Regime
		d (mm)	δ (cm)	ΔT(°C)	
Manzello et al.	[21]	3.1 ± 0.1	1	120–160	Vapor explosions
Lan et al.	[19]	1.8–2.4	≈ 5	120	Vapor explosions
Alchalabi et al.	[1]	1	10	≈100–200	Vapor explosions
Present study	–	2.2	0.1–0.3	≳ 60	Vapor explosions
Present study	–	2.2	0.1–0.3	30–50	Jetting regime

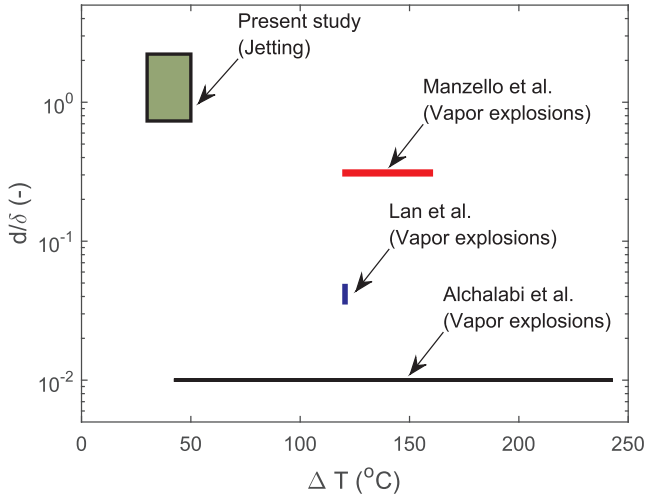

Fig. 2. Parameter space of the present study and those from Refs [1; 20; 21].

speed, break-up time and satellite droplet sizes. The reader should keep in mind that this jet was only observed in a relatively narrow parameter space, principally governed by the oil temperature, $T_o \approx 130$–150 °C, i.e. $\Delta T \approx 30$–50 °C.

Table 2
Physical properties of the test liquids.

Liquid	Density ρ (kg/m^3)	Viscosity μ (mPa s)	Surface tension σ (mN/m)
Water	1000	1	72
Canola oil ($T_o = 20$ °C)	920	66	33.8
Canola oil ($T_o \approx 150$ °C)	850	5	33.8

2. Materials and methods

Fig. 3 presents an overview of the experimental configuration; Oil is placed in a well of depth $\delta = 1$, 2 or 3 mm, in an Aluminium plate, which is situated on a hot plate. The oil film temperature is monitored by a K-type thermocouple probe (fully immersed in the oil film) and we do not release the water droplet until the temperature reads a steady temperature, T_o, for at least 1 min. The water is injected by the impingement of a droplet from a hydrophobized glass capillary 10 cm above the plate. The pinch-off of the droplet from the capillary is highly reproducible with diameter $d = 2.2$ mm (volume $V \approx 5.7\mu$L), so we have a repeatable droplet volume for each trial. From this release height, the

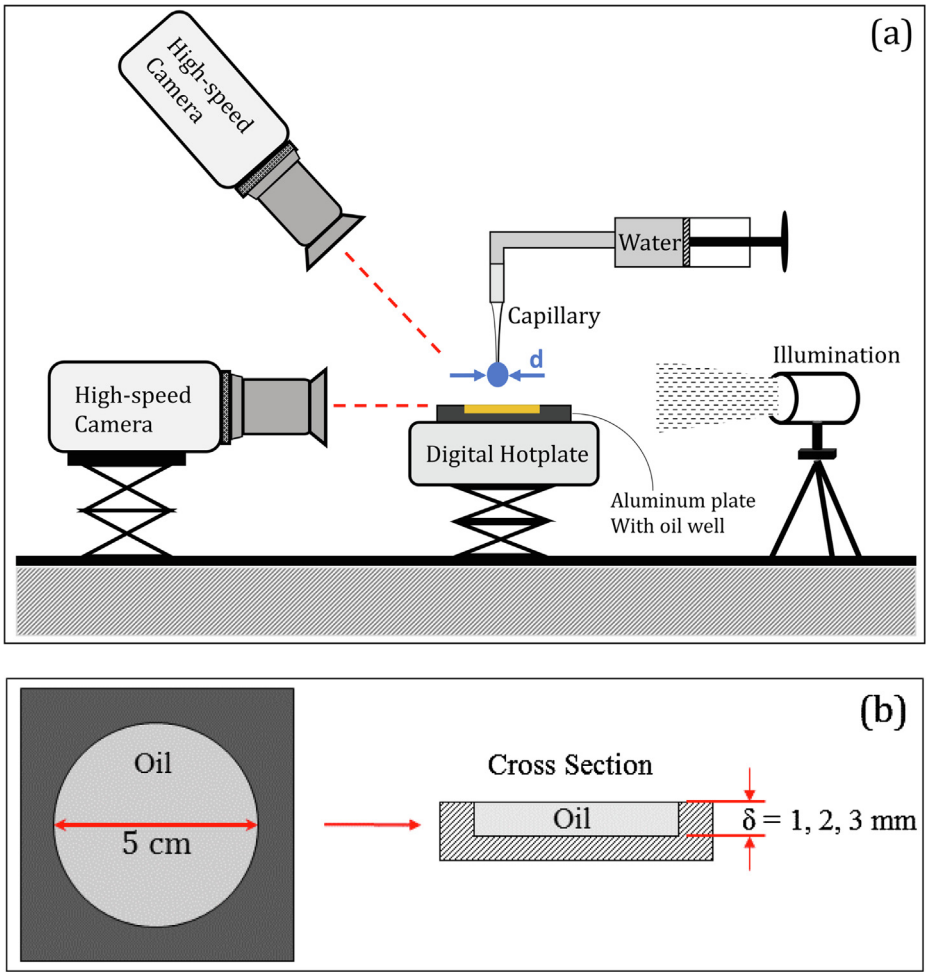

Fig. 3. Schematic representation of the experimental setup showing (a) Camera orientation and droplet injection, and (b) target plate and oil well dimensions.

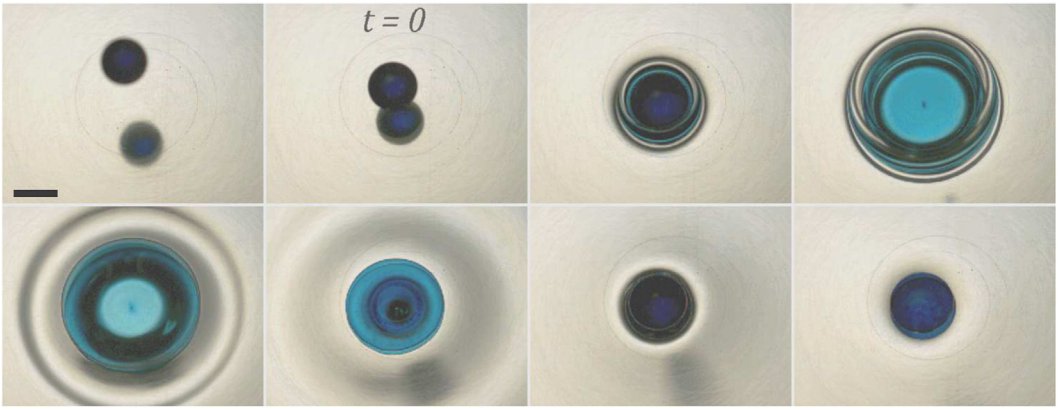

Fig. 4. Example image sequence taken from a high-speed video of the impact dynamics. The top row shows the impact and spreading, whilst the bottom row shows the retraction toward the final state. Frames are taken at $t = -5.3$, 0, 3.3, 10, 21.3, 36.3, 61, 113.6 ms.

impact speed is $V_i = \sqrt{2gh} \approx 1.4$ m/s, and the impact Weber number is $We = \rho d V_i^2/\sigma \approx 54$. As such, the impact does not causes a splash, and the droplet does not fragment (i.e. remains intact as a single volume), as depcited by the image sequence in Fig. 4.

The imaging system consists of two high-speed cameras and background illumination by an LED array and diffuser screen. The cameras (Phantom Miro 310 and Phantom V711) are frame-synchronized and triggered manually (with a center-based trigger) upon human detection of the first vaporization event. Using micro-Nikkor lenses, the effective pixel resolution of the cameras was between 50 and 100 μm/px and we used frame rates up to 20,000 fps, yielding a temporal resolution of 50 μs.

The physical properties of both water and the oil at ambient lab temperature (22 °C) are given in Table 1, however, due to heating, we estimate the true effective viscosity and density of the oil from previous literature measurements [31] as $\mu \approx 5$ mPa s and $\rho \approx 850$ kg/m^3.

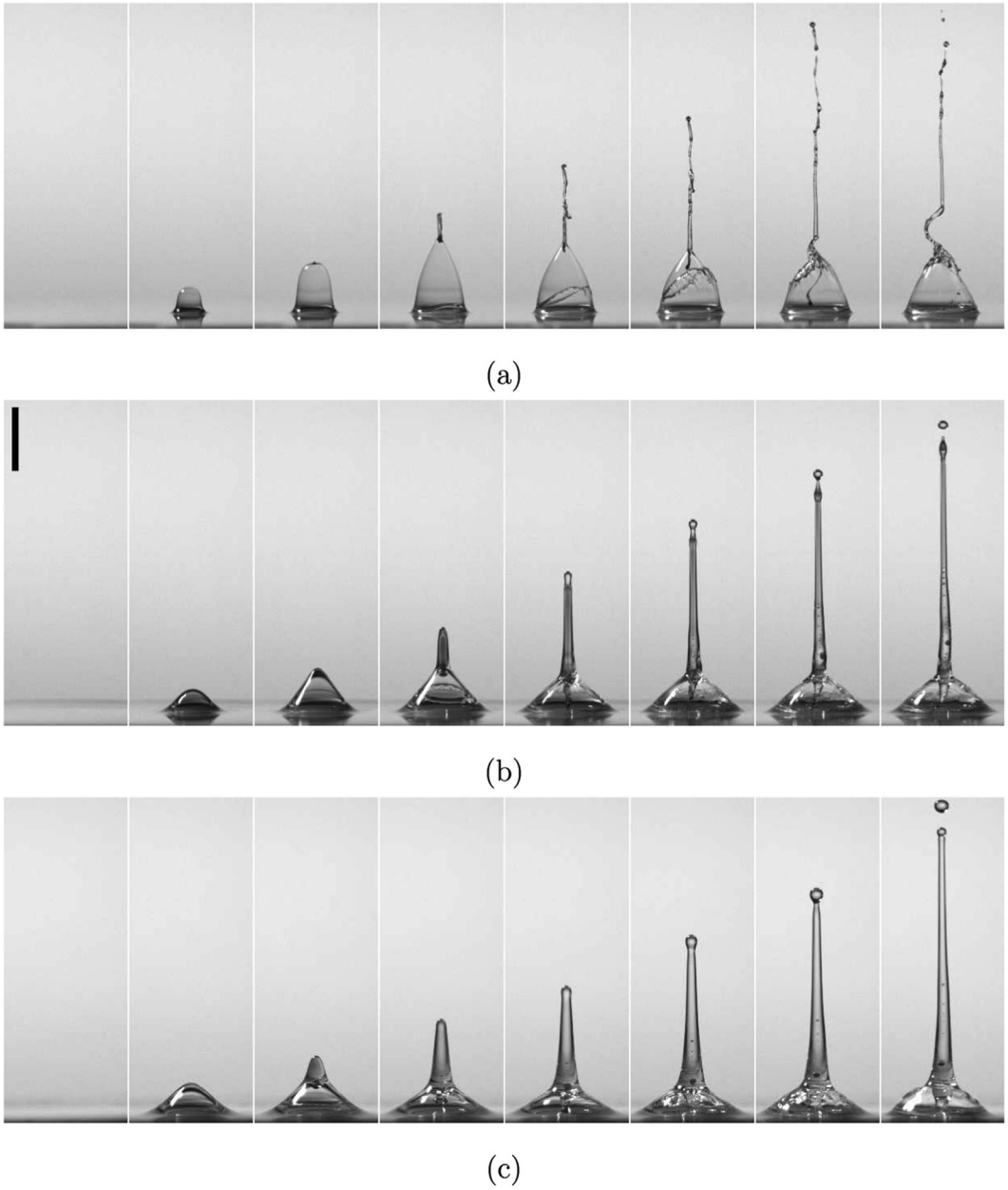

Fig. 5. Side view of the partial vaporization process for (a) $\delta = 1$ mm ($t = 0$, 0.5, 1, 2, 3, 4, 6, and 8 ms) , (b) $\delta = 2$ mm ($t = 0$, 1, 2, 4, 7, 10, 13, and 16 ms), and (c) $\delta = 3$ mm ($t = 0$, 2, 4, 6, 10, 15, 20, and 30 ms). The scale bar in (b) indicates 1 cm and the times are relative to the start of the vaporization process. The oil film temperature in all cases was $T_o = 130$ ˚C.

3. Results and discussion

3.1. Qualitative overview

For purposes of a qualitative overview of the dynamics, we present the reader with three representative image sequences in Fig. 5(a)–(c), depicting the evolution of a jet rising out of a hot oil film. These are typical sequences observed where the primary control parameter is the oil film thickness, which was varied from $\delta = 1$ mm in (a) to $\delta = 3$ mm in (c). For comparison, the oil film temperature, as read by the thermocouple was constant at $T_o = 130$ ˚C in all cases. The key difference between the sequences are timescales (see figure for exact times), whereby the dynamics occur over a relatively short timescale for $\delta = 1$ mm, with jet break-up occurring at $t \approx 4$ ms. With an increase in film thickness, however, the jet break-up does not occur until $t \approx 25$ ms for $\delta = 3$ mm.Specific to Fig. 5(a), the final images at $t = 6$–8 ms indicate a disturbance to the base of the jet. This is related to retraction of the water film inside the dome, discussed in Section 3.4.

Irrespective of timescale, the mechanism behind the jet is the same in all cases; The expansion of a vapor bubble below the oil film initiates fluid flow in both the radial and vertical directions. As the bubble expands vertically, the oil film converges at the apex of an axisymmetric dome-shape and focuses to create a jet-flow. In fact, as will be shown later, this focusing creates both an upward-facing jet and a downward-facing re-entrant jet. Interestingly, the upward-facing jet is comprised primarily of oil, whilst the downward-facing jet is primarily water. However, there are some cases where we observe water entrained into the upward jet (see Section 3.4). It is precisely because of the mechanism behind the jet, i.e. vapor bubble expansion, that it is only observed for a relatively small parameter range; If the oil temperature is too high above the boiling point of the droplet, then the vaporized volume and bubble expansion rate are large enough to rupture the film

violently, resulting in explosive vaporization (e.g. Fig. 1(a)). Note also that only a fraction of the water droplet is vaporized during the initial expansion and jet formation, and the remainder of the water lines the inside of the vapor dome (see Section 3.4).

From just a brief visual inspection of these sequences, some stark differences are observed as the film thickness is increased. The effect of timescale notwithstanding, these are: (i) The vapor 'dome' shape is vastly different for the thinnest film and promotes extended growth in the vertical direction before the jet emerges, whilst for the thicker films, the vapor bubble below the surface expands farther in the horizontal plane. (ii) The jet diameter increases with film thickness and thus delays the break-up time and increases the size of primary satellite droplets. (iii) The entrainment of water into the upward-facing jet (see image 4 in Fig. 5(b) for example) qualitatively changes with film thickness. Each of these three primary observations are addressed in more detail in the subsections below, along with one additional observation made only for the thickest films – namely – secondary vaporization.

3.2. Vapor dome

The time-resolved image sequences in Fig. 5 show that the fluid motion is initiated by the growth of a vapor bubble, which is submerged in the hot oil film. This expanding vapor bubble pushes fluid upward, which converges at the apex of a dome or conical structure. This dome expands both radially and vertically in the early stages before the emergence of the jet, and the shape is dictated by the film thickness. To demonstrate this, Fig. 6(a)–(c) present snapshots of vapor domes at $t = 2$ ms for the different film thicknesses.

To quantitatively analyze the differences in the growth of the vapor bubble and the ensuing jet, we implemented simple edge-finding routines, an example of which is shown in Fig. 7(a). For clarity, all times are stated relative to the onset of vaporization, which is more precisely determined by the angled camera view. However, as seen in the data in Fig. 7(b), the vapor dome does not appear above the initial free surface until approximately 100–200 μs, hence data does not track to the origin ($t = 0$). Keep in mind also that the limit of the base diameter for practical measurements is that of the submerged drop, i.e. $d_{base}|_{t=0} \approx 2.5$ mm, which is measured from the inclined view. Due to the modified interfacial tension between the water and the oil, $\sigma_i \approx 25$ mN/m, the effective capillary length is $l = \sqrt{\sigma_i/(\Delta\rho g)} \approx 5.6$ mm. Therefore, the submerged droplet does not deform significantly due to the presence of the surrounding oil, but may experience some degree of 'flattening' due to the impact, resulting in an effective diameter larger than the original droplet ($d = 2.2$ mm).

For the specific realization in Fig. 7, we observe a rapid growth of the base diameter for $t \lesssim 1$ ms, corresponding to the initial vapor bubble growth. The dome continues to expand for $t > 2$ ms, but at a significantly reduced rate and plateaus at $d_{base} \approx 17$ mm for $t \gtrsim 4$ ms. The jet, on the other hand, exhibits a more steady growth, and we could reasonably fit a linear function to the data for $t \gtrsim t_{jet} = 2.8$ ms, i.e. the jet emergence time, which provides an estimate of the initial jet speed as $v_{jet} \approx \Delta h/\Delta t$, which gives the initial jet speed of $v_{jet} \approx 2.08$ m/s.

The same image analysis routine was performed across all the trials for different thicknesses, and the summarized data is presented in Fig. 8(a)–(c), plotted up to the approximate time of jet break-up. By inspection of the data for both height and diameter across the different film thickness, the visual trend in Fig. 4 is confirmed; The dome is taller and approximates a conical shape for the thinnest film ($\delta = 1$ mm), and is broader with a significantly suppressed profile for the thickest film ($\delta = 3$ mm).

With regards to the principal timescale, i.e. the time of jet emergence, t_{jet}, we observe that it increases monotonically with film thickness. Our data, encompassing multiple repeat trials indicate that $t_{jet} = 1.62 \pm 0.27$ ms, 2.17 ± 0.57 ms, and 3.04 ± 0.27 ms for film thicknesses of $\delta = 1$ mm, 2 mm and 3 mm, respectively. For reference, the mean jet emergence times are marked by the vertical dashed lines in Fig. 8(a)–(c).

In all cases, we observe a similar qualitative trend as in Fig. 7(b), with a rapid expansion of the vapor bubble primarily in the horizontal direction in the early stage, then a plateau in both diameter and height of the vapor dome. The jet, however, progresses more steadily until break-up, as seen in the curves for jet height. Again, by taking the slope of the height-time curves forward from the point of jet emergence, we extract the following mean jet speeds, where we have used a time step of $\Delta t = 1$ ms in all cases for consistency: $v_{jet} = 5.97$ m/s, 2.98 m/s, and 1.68 m/s for $\delta = 1$, 2, and 3 mm respectively. The linear fit across this time step is excellent in all cases with $R^2 > 0.99$, however the best fit across the entire span of the data is given by a simple power-law, $h \sim t^{\beta} \Rightarrow v_{jet} = dh/dt \sim t^{\gamma}$, where $\gamma = \beta - 1$. For example, this analysis gives an approximate relation of $h \sim t^{0.8}$ and $v_{jet} \sim t^{-0.2}$ for $\delta = 3$ mm, but this cannot be reconciled with any physical arguments at present.

As a final observation, from a statistical standpoint, the data in Fig. 8(a), exhibits a higher degree of intra-sample variation compared to Fig. 8 (b) and (c), especially around t_{jet}, when the jet emerges. We rationalize this to the variation in film thickness, during preparation of the experiment, whereby the oil film thickness is set by adding a specific volume into the well to fill to the level. The variation therefore diminishes (in terms of absolute difference in film thickness, i.e. $\delta - \bar{\delta}$) as the film thickness increases from 1 mm to 3 mm. This systematic

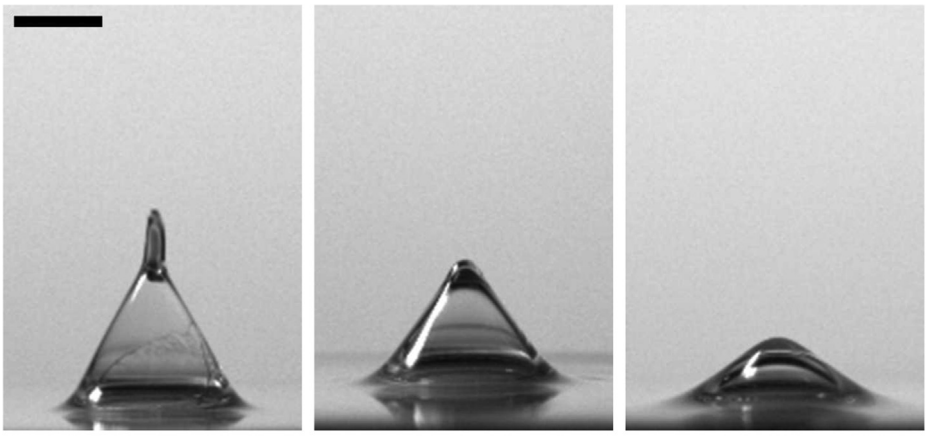

Fig. 6. Snapshots of the vapor dome viewed from the side at $t = 2$ ms for (a) $\delta = 1$ mm, (b) $\delta = 2$ mm, and (c) $\delta = 3$ mm. The scale bar in (a) represents 5 mm.

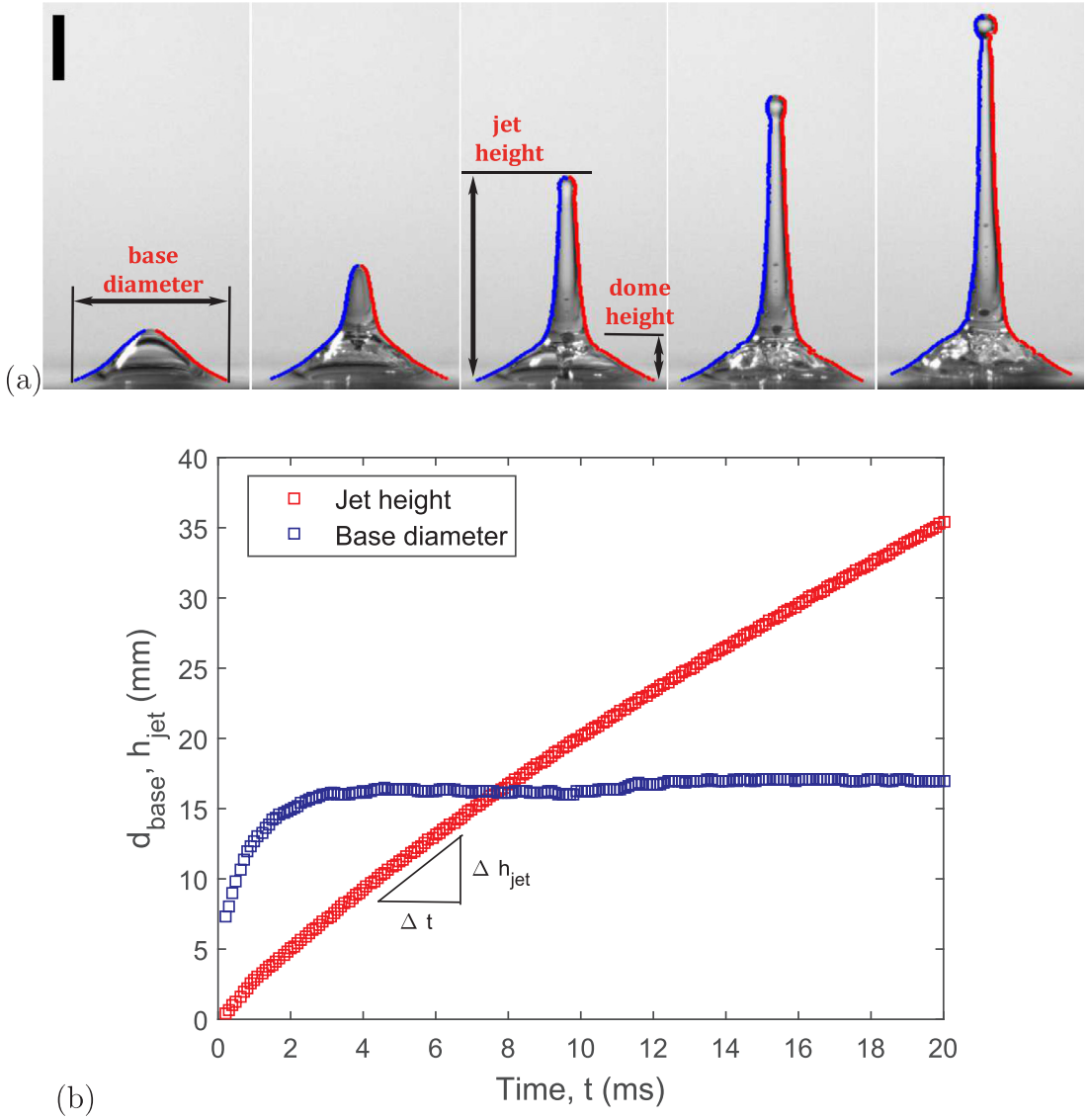

Fig. 7. (a) Example of image analysis to extract the vapor dome and jet profile for times t = 2, 5, 10, 15, and 20 ms. The blue and red lines outline the left and right edges, respectively. (b) The plot below shows the extracted characteristics – namely – base diameter and jet height up to t = 20 ms, close to the jet break-up. δ = 3 mm, T_o = 130 C. The slope of the jet height marked next to the data estimates the jet speed, v_{jet}. (For interpretation of the references to colour in this figure legend, the reader is referred to the web version of this article.)

variation notwithstanding, the overall trends and qualitative differences in the data for increasing film thicknesses are clear – namely – the dome shape is more conical for thinner films and broader for thicker films. Furthermore, the jet emergence time increases with film thickness whilst the initial jet speed decreases.These observations can be reconciled to the fact that the vapor bubble growth is resisted by thicker films; liquid in the film must first be drained from the vicinity of the vapor bubble in order for the dome and jet to grow vertically, which occurs over an exaggerated timescale for thicker films. Likewise, the thicker film leads to a thicker jet base, and hence from a momentum perspective, assuming equal energy from the sudden onset of the vaporization, the jet must be slower since more mass is entrained into the jet flow.

3.3. Jet break-up and droplet sizes

The jet propagation is sustained by momentum as fluid is drawn into the vertical column from the film around the jet base and, over the timescales of the experiment, the dynamics are not governed by viscous forces. This can be confirmed by assessing the jet Reynolds numbers; Taking the viscosity and density of the heated oil as $\mu \approx 5$ mPa s and $\rho \approx 850$ kg/m^3, $\delta \approx 1$–3 mm and $v_{jet} \approx 2$–5 m/s, we have the following estimate:

$$Re = \rho \delta v_{jet}/\mu \approx \mathcal{O}(10^2 - 10^3) \tag{1}$$

The jet tapering and break-up are therefore governed by fluid inertia and capillary forces. This is also clear if we calculate the characteristic capillary timescale, using δ as the relevant lengthscale and $\sigma \approx 33$ mN/m,

$$\tau = \sqrt{\frac{\rho \delta^3}{\sigma}} \approx 5\text{–}26 \text{ ms} \tag{2}$$

which is in excellent agreement with the observed break-up times from the raw video data (see Fig. 4). The choice of δ as the relevant lengthscale is supported by inspection of the jet diameters (e.g. Fig. 4), which scales monotonically with δ.

The surface tension-driven break-up of the jet leads to the ejection of multiple satellite droplets. To analyze the distribution of these droplet sizes, a simple calculation based on area, A, of the binarized droplet

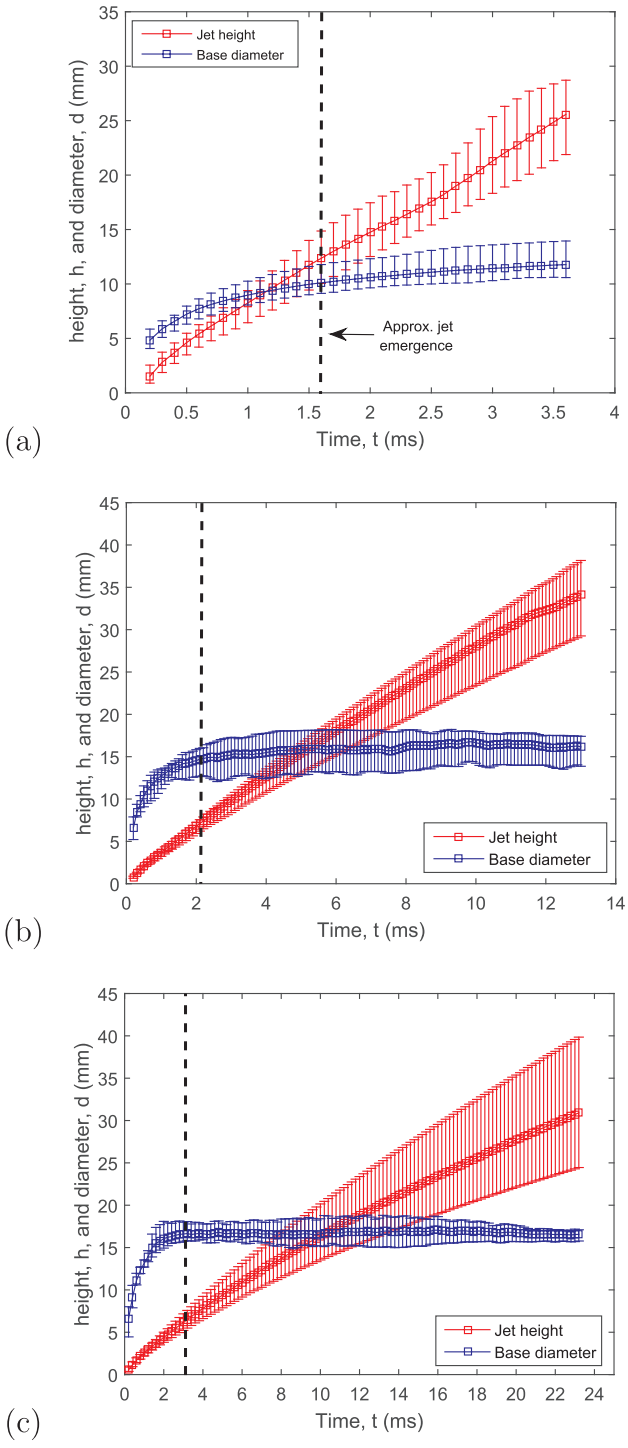

Fig. 8. Base diameters and jet heights for (a) $\delta = 1$ mm, (b) $\delta = 2$ mm, and (c) $\delta = 3$ mm. In each plot, the data point at any given time represents the mean of all repeat trials (minimum of three), whilst the error bars encompass the total range. Data is plotted up to the approximate time of jet break-up. The vertical dashed lines indicate the time that the jet emerges from the top of the vapor dome.

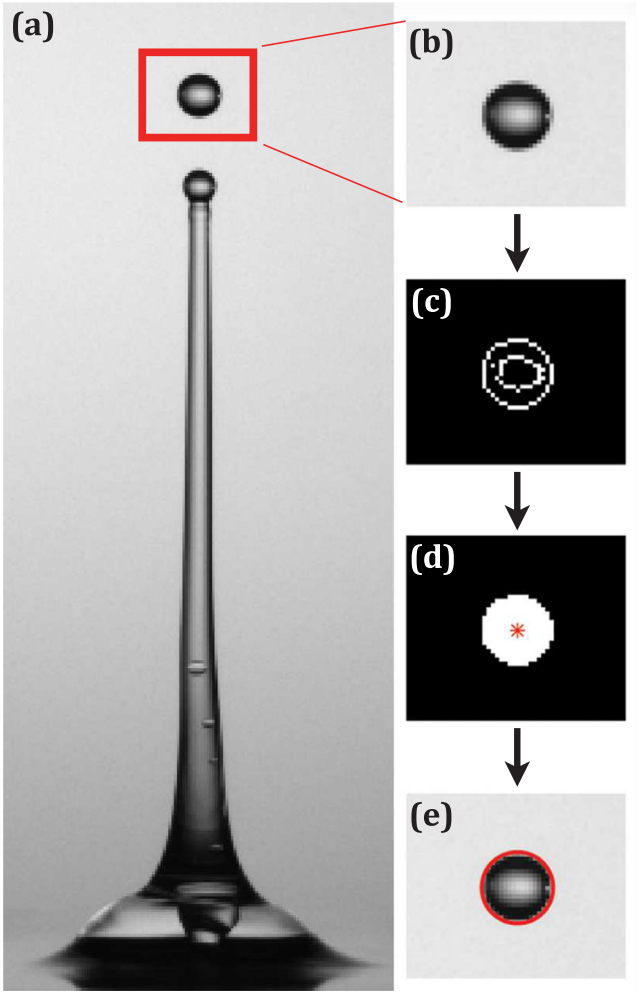

Fig. 9. Graphic depicting the image processing for extracting satellite droplet sizes. (a) Raw full image, (b) Cropped region around the satellite droplet, (c) Application of a binary gradient mask, (d) Filled binary image with the centroid marked by red star, and (e) Cropped raw image with perimeter (in red) based on the centroid and circular equivalent radius, $r = \sqrt{A/\pi}$ from the binarized image in (d). (For interpretation of the references to colour in this figure legend, the reader is referred to the web version of this article.)

was performed to give the primary satellite as $d_1 = 2r_1 = 2\sqrt{A/\pi}$,where d_1 is the diameter and r_1 is the radius of the primary satellite droplet. The steps used in this calculation are shown in Fig. 9.

Performing this procedure over all the trials with primary satellite droplets, yields the raw droplet sizes shown in Fig. 10(a), where we find the total range of all droplets is approximately 0.8–3.5 mm. Given that the jet arises from the top of the vapor dome, which pushes the entire oil film upward, we expect that the jet base diameter, d_0, should be approximately equal to the film thickness. In turn, given that the jet breakups herein are in the Rayleigh regime [20], the satellite droplets should also be of the order of the film thickness, i.e. $d_1 \sim d_0 \sim O(\delta)$. This is confirmed by the data in Fig. 10(a). However, we also find that the *relative* droplet sizes are inversely correlated to film thickness. This can be shown by examining the normalized droplet diameters, d_1/δ, shown in Fig. 10(b), where the median droplet sizes normalized by the film thickness are $\widetilde{d_1}/\delta \approx 1.1$, 0.85, 0.667 for $\delta = 1$, 2, and 3 mm respectively. Given this discretization of drop sizes for both the raw and normalized data, we perform distribution fits on the individual data sets, rather than the ensemble data, and plot the cumulative distributions in Fig. 10(c). The experimental data for each individual film thickness exhibit an approximately normal distribution, as shown by the fitted curves for each data set, determined by the parameters $(\hat{\mu}, \hat{\sigma}) = (1.106, 0.194)$, (0.879,0.092) and (0.693, 0.096), respectively, which again shows a higher degree of variation for the thinnest film.

Previously, for jets emanating from orifices with fixed diameter, $d_0 = 1$–3 mm, with a fixed flow rate (e.g. [36]), it was found that the median primary droplet diameters were larger than the orifice, i.e. $d_1/d_0 > 1$, however the exit speeds were less than 1 m/s yielding a Weber number $We = \rho d_0 V_0^2/\sigma = O(1)$. In contrast, in our experiment,

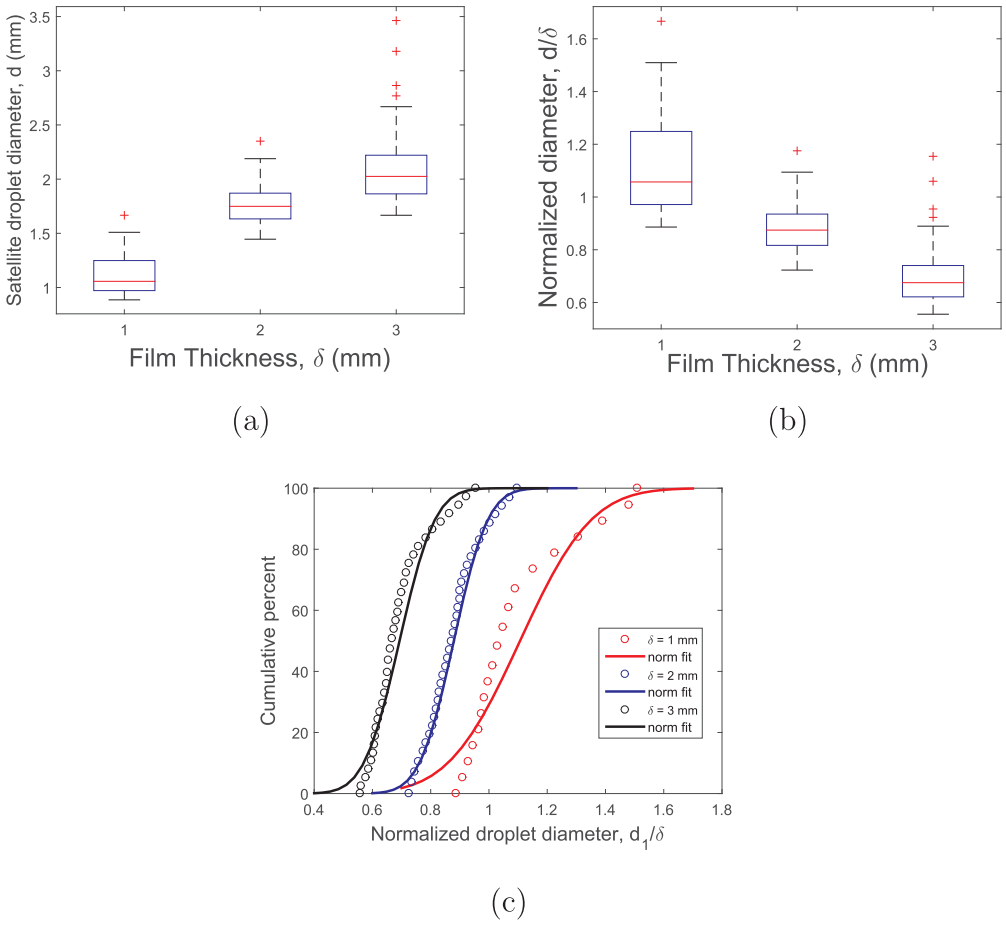

Fig. 10. (a) Boxplot Summaries of droplet sizing for each of the different film thicknesses, with outliers indicated by the red crosses. (b) Data (excluding outliers) normalized by corresponding film thicknesses, d_1/δ.

although initial diameters are comparable, the jet mechanism is fluid focusing at the top of a vapor dome and our observations are for a significantly different parameter regime, with the relevant Weber number defined as $We_\delta = \rho\delta v_{jet}^2/\sigma = O(100\text{–}1000)$.

For primary satellite droplets, shed from the tip of the jet, the initial jet momentum sustains flow into the tip region, whilst surface tension decelerates the tip slightly, which leads to fluid accumulation in the end region. The analytical description of this process, given by Gordillo and Gekle [16], predicts that the normalized drop size scales inversely with the jet Weber number based on axial strain, given in their work as $\hat{r} \propto We_s^{-1/7}$, where $We_s = \rho R_0^3 S_0^2/\sigma$ with S_0 being the axial strain. From our experimental data, our best fit of the normalized drop size to Weber number is given by $\widetilde{d_1}/\delta \propto We_\delta^{-0.35}$, which confirms the inverse correlation albeit with a different power-law exponent. However, further experimental studies from different parameter regimes and jet production mechanisms will be needed to validate this inverse Weber number correlation.

3.4. Compound jets, water 'peeling' and secondary vaporization

In some cases, we observed that the jet flow caused water entrainment into the main jet. An example of this phenomenon is shown in Fig. 11 for a 2 mm oil film, where both the dye and the difference in refractive index permits distinction between water and oil phases. In this case, the nucleation point for the vaporization is central relative to the water droplet so that the expanding vapor bubble symmetrically displaces both the water and the oil film. As such, when the flow focuses at the apex of the conical vapor dome, the upward momentum in the oil jet entrains water, creating a compound water-oil jet, as seen in the final panel of Fig. 11(a). As the jet evolves, the axial extension of this compound structure leads to the disintegration of the water into discrete droplets and threads, which is seen in the later-time snapshot in Fig. 11(b). In this specific realization, the primary satellite droplet consists of pure oil, whilst the secondary droplet is a compound droplet. The fact that the water thread encapsulated in the oil jet does not vaporize indicates that the presence of the solid plate is essential for initiating the vaporization in our range of superheat temperatures ΔT = 30–50 °C.

Focusing again on the final panel in Fig. 11(a), we also observe the evolution of a downward-facing re-entrant jet, which is marked by the red arrow. This was also observed experimentally by Brown et al. [8] and Brasz et al. [37], albeit at a smaller scale. In their experiment, the vapor dome was initiated by a laser-pulse and the fluid was single-phase. However, the re-entrant jet in the case of laser-induced cavities appears to be attributed more to the collapse of a cavity in the proximity of a solid wall (e.g. [4,6,9,28]).

In contrast, the formation of the re-entrant jet in our experiment has more to do with the principal mechanism – namely – flow separation at the apex of the dome. It is interesting to note that the composition of the two jets is different, in that the downward-facing jet consists primarily of water, at least in the early stage. This discrepancy can be understood by noting that a secondary mechanism is at play, which is more relevant to the downward facing jet; We describe this mechanism as water 'peeling' from the oil inside the vapor dome, as depicted by the schematic diagram in Fig. 12(a). For clarity, the outer oil surface is shown in gold, whilst the inner water surface is blue and the interface is black. We hypothesize that this peeling is driven by the surface tension of the water, from which we can estimate the thickness of the water film

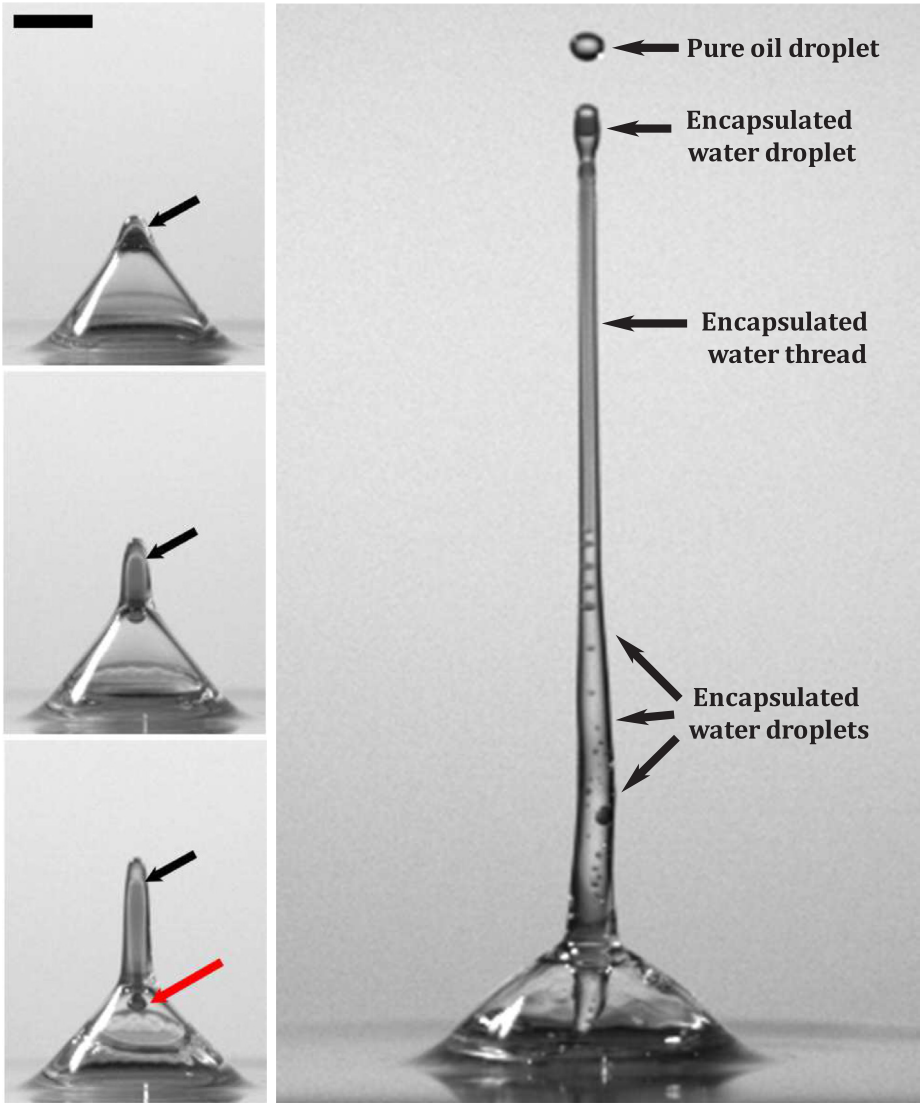

Fig. 11. (a) Image sequence showing the entrainment of water into the upward jet. Black arrows indicate the top of the water column encapsulated in the oil, whilst the red arrow in the third panel indicates the start of the downward-facing water column inside the vapor dome. Images are separated by 1 ms and the scale bar is 5 mm. (b) Snapshot taken later in the same realization (t = 17 ms) showing the result of the compound structure disintegration. (For interpretation of the references to colour in this figure legend, the reader is referred to the web version of this article.)

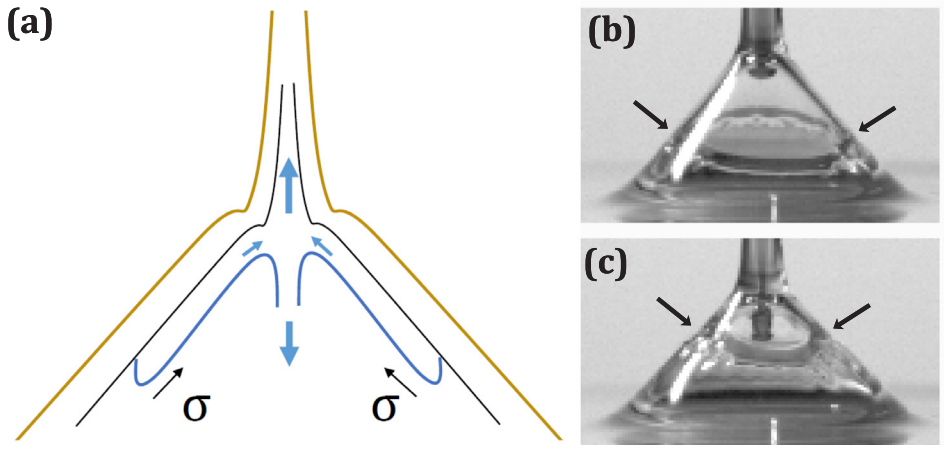

Fig. 12. (a) Schematic of proposed 'peeling' mechanism showing the interface between water and oil in black and the surface-tension driven peeling in blue. (b)and (c) Zoomed images, separated by 1 ms, of the peeling with arrows indicating the extent of the retracting water. (For interpretation of the references to colour in this figure legend, the reader is referred to the web version of this article.)

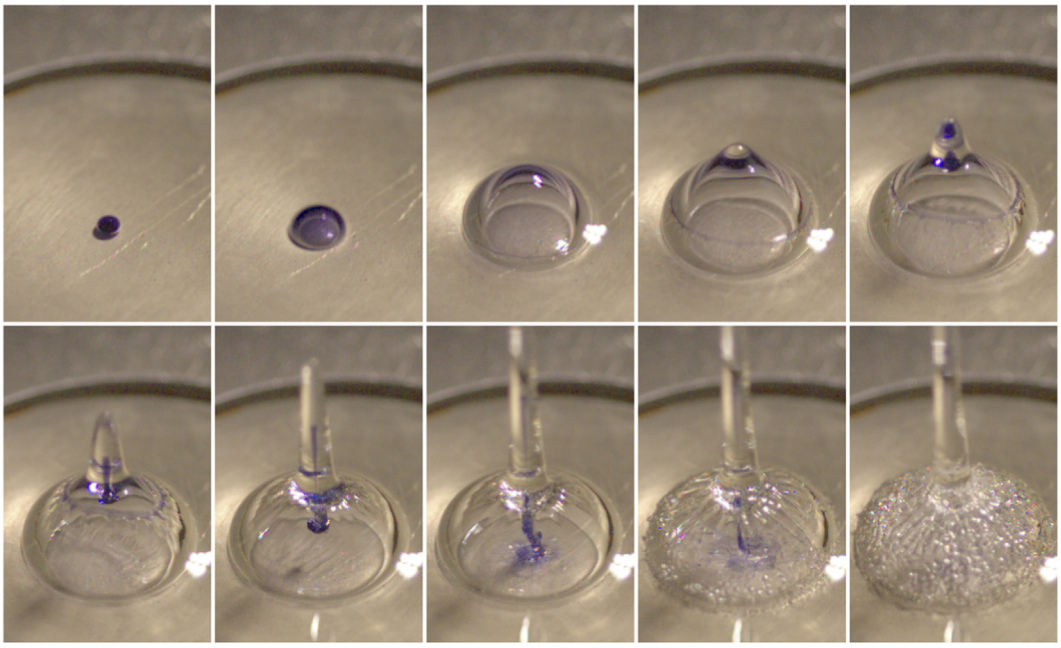

Fig. 13. Inclined camera view of the secondary vaporization process for $\delta = 3$mm, $T_o = 150$ °C.The water droplet is blue, whilst the clear liquid is the oil. The times from the first motion due to vaporization are $t = -0.1$, 0.3, 1.3, 2.3, 3.3, 4.3, 6.3, 8.3, 9.3, and 10.3 ms. See also the supplemental video for this figure. (For interpretation of the references to colour in this figure legend, the reader is referred to the web version of this article.)

inside the dome using the well-known Taylor-Culick law for retracting free-surfaces. By tracking the extent of the water edge (marked by the black arrows in Fig. 12(b) and (c)) in a number of different trials we find that the retraction speed is consistently around 2 m/s. From this, the Taylor-Culick law yields the film thickness as $2\sigma/(\rho v_{TC}^2) \approx 40\mu$m. This estimate is reasonable if we consider that the approximate conical surface area of the vapor dome is $O(10^{-4})$ m^2 and the volume of the droplet is $O(10^{-9}$–$10^{-8})$ m^3, giving an evenly distributed film of 10–100 μm.

The final observation in this process occurs when the downward-facing jet (comprised of water) makes contact with the bare hot plate inside the expanded vapor dome. A top-view color sequence of this is shown in Fig. 13. Water striking the hot plate causes prompt splashing and a spray of fine droplets inside the vapor dome, which distorts the interface and creates a rough appearance on the outer surface. This secondary vaporization results in the release of small oil droplets near the base of the jet, and disturbs the jet flow, but does not affect the first jet breakup. The sudden expulsion of small droplets is an example of thermal atomization, which has been reported many times in the context of droplet impact on a solid surface (e.g. [35,30]). In our case, where the thermal atomization occurs within the confinement of an oil dome, vapor is also formed and the oil dome base undergoes several oscillations (see video).

4. Conclusions

Herein we have presented observations from an experimental study of the vaporization of water droplets submerged in a hot oil film. Our high-speed video imaging has revealed several interesting features associated with this process, the foremost of which is a vertical jet which emerges from the apex of a 'vapor dome'. A fraction of the submerged water droplet vaporizes and rapidly expands, which pushes the surrounding oil film vertically and radially away from the site of nucleation. As the expansion slows, fluid converges at the apex of the vapor bubble and focuses to create both an upward vertical jet and a downward re-entrant jet. The upward-moving jet is primarily oil, but in some cases entrains a water column to create a compound jet structure. The re-entrant jet consists primarily of water due to the supplemental mechanism we have identified as water 'peeling', where the remaining water droplet retracts inside the vapor dome due to surface tension. When this re-entrant jet strikes the naked hot plate, it causes a secondary vaporization event that sends a fine spray of droplets into the vapor dome and distorts the oil interface.

The jet mechanism is qualitatively similar to previous studies on laser-induced jets, whereby a focused laser pulse below a free-surface creates a vapor bubble that expands rapidly and results in both a jet moving away from the free-surface and a re-entrant jet into the vapor.

The primary vertical jet is governed by fluid inertia and capillary forces, and the breakup time agrees very well with the characteristic capillary timescale, $\sqrt{\rho\delta^3/\sigma}$. At the break-up point, a primary satellite droplet is ejected and is of the order of the oil film thickness, with $d_1 \approx 0.8$–3.5 mm, however the normalized median droplet diameters are inversely correlated to film thickness, i.e. $d_1/\delta \propto 1/\delta$. Future studies could expand upon the range of thicknesses studied herein to bridge the gap between films and deeper pools, as studied by Manzello et al. [21].

In terms of the principal control parameter, i.e. oil film temperature, our observations of this novel jet mechanism were in restricted parameter space with $T_0 \approx 130$–150°C. Above this range, the vaporized volume increases and the vapor bubble expansion occurs so rapidly that the oil films rupture before the emergence of a jet. This high-temperature regime is therefore characterized by a violent fragmentation process, which presents significant experimental challenges and is to be the subject of a subsequent publication.

Declaration of Competing Interest

The authors declared that there is no conflict of interest.

Appendix A. Supplementary material

Supplementary data associated with this article can be found, in the online version, at https://doi.org/10.1016/j.expthermflusci.2019.109873.

References

[1] M.A. Alchalabi, N. Kouraytem, E.-Q. Li, S.T. Thoroddsen, Vortex-induced vapor explosion during drop impact on a superheated pool, Exp. Therm. Fluid Sci. 87 (2017) 60–68.
[2] A. Antkowiak, N. Bremond, S. Le Dizes, E. Villermaux, Short-term dynamics of a density interface following an impact, J. Fluid Mech. 577 (2007) 241–250.
[3] D. Bartolo, C. Josserand, D. Bonn, Singular jets and bubbles in drop impact, Phys. Rev. Lett. 96 (2006) 124501.
[4] T.B. Benjamin, A.T. Ellis, Collapse of cavitation bubbles and pressures thereby produced against solid boundaries, Phil. Trans. R. Soc. Lond. Ser. A 260 (1966) 221–240.
[5] R. Bergmann, D. van der Meer, A. van der Bos, D. Lohse, Controlled impact of a disk on a water surface: cavity dynamics, J. Fluid Mech. 633 (2009) 381–409.
[6] J.R. Blake, D.C. Gibson, Cavitation bubbles near boundaries, Annu. Rev. Fluid Mech. 19 (1987) 99–123.
[7] C.F. Brasz, J.H. Yang, C.B. Arnold, Tilting of adjacent laser-induced liquid jets, Microfluid Nanofluid 18 (2015) 185–197.
[8] M.S. Brown, N.T. Kattamis, C.B. Arnold, Time-resolved dynamics of laser-induced micro-jets from thin liquid films, Microfluid Nanofluid 11 (2011) 199–207.
[9] E.A. Brujan, K. Nahen, P. Schmidt, A. Vogel, Dynamics of laser-induced cavitation bubbles near an elastic boundary, J. Fluid Mech. 433 (2001) 251–281.
[10] R.C.C. Chen, T.T. Yu, K.W. Su, J.F. Chen, Y.F. Chen, Exploration of water jet generated by Q-switched laser induced water breakdown with different depths beneath a flat free surface, Opt. Express 21 (2013) 445–453.
[11] V. Duclaux, F. Caille, C. Duez, C. Ybert, L. Bocquet, C. Clanet, Transient cavities, J. Fluid Mech. 591 (2007) 1–19.
[12] J. Eggers, E. Villermaux, Physics of liquid jets, Rep. Prog. Phys. 71 (2008) 036601.
[13] D.L. Frost, Dynamics of explosive boiling of a droplet, Phys. Fluids 31 (1988) 2554–2561.
[14] S. Gekle, J.M. Gordillo, Generation and breakup of Worthington jets after cavity collapse. Part 1. Jet formation, J. Fluid Mech. 663 (2010) 293–330.
[15] E. Ghabache, T. Seon, A. Antkowiak, Liquid jet eruption from hollow relaxation, J. Fluid Mech. 761 (2014) 206–219.
[16] J.M. Gordillo, S. Gekle, Generation and breakup of Worthington jets after cavity collapse. Part 2. Tip breakup of stretched jets, J. Fluid Mech. 663 (2010) 331–346.
[17] C.J. Gurney, M.J.H. Simmons, V.L. Hawkins, S.P. Decent, The impact of multi-frequency and forced distrubances upon drop size distributions in prilling, Chem. Eng. Sci. 65 (2010) 3474–3484.
[18] S.D. Hoath, E.P. Furlani, Fluid mechanics for inkjet printing, in: S.D. Hoath (Ed.), Fundamental of Inkjet Printing, Wiley, 2016, pp. 13–53.
[19] M. Lan, X. Wang, P. Zhu, P. Chen, Experimental study on the dynamic process of a water drop with additives impact upon hot liquid fuel surfaces, Energy Proc. 66 (2015) 173–176.
[20] S.P. Lin, R.D. Reitz, Drop and spray formation from a liquid jet, J. Fluid Mech. 30 (1998) 85–105.
[21] S.L. Manzello, J.C. Yang, T.G. Cleary, On the interaction of a droplet with a pool of hot cooking oil, Fire Safety J. 38 (2003) 651–659.
[22] J.O. Marston, S.T. Thoroddsen, Apex jets from impacting drops, J. Fluid Mech. 614 (2008) 293–302.
[23] J.O. Marston, M.M. Mansoor, S.T. Thoroddsen, T.T. Truscott, The effect of ambient pressure of ejecta sheets from free-surface ablation, Exp. Fluids 57 (2016) 61.
[24] G.D. Martin, S.D. Hoath, I.M. Hutchings, Inkjet printing – the physics of manipulating liquid jets and drops, J. Phys: Conf. Ser. 105 (2008) 012001.
[25] M. Moradiafrapoli, J.O. Marston, High-speed video investigation of jet dynamics from narrow orifices for needle-free injection, Chem. Eng. Res. Des. 117 (2017) 110–121.
[26] L. Partridge, D.C.Y. Wong, M.J.H. Simmons, E.I. Parau, S.P. Decent, Experimental and theoretical description of the break-up of curved liquid jets in the prilling process, Chem. Eng. Res. Des. 83 (2005) 1267–1275.
[27] J. Plateau, Statique Experimentale et Theorique des liquides, Gauthier-Villars, 1873.
[28] S. Popinet, S. Zaleski, Bubble collapse near a solid boundary: a numerical study of the influence of viscosity, J. Fluid Mech. 464 (2002) 137–163.
[29] W.S. Rayleigh, On the instability of jets, Proc. Lond. Math. Soc. 306 (1878) 145–165.
[30] I.V. Roisman, J. Breitenbach, C. Tropea, Thermal atomization of a liquid drop after impact onto a hot substrate, J. Fluid Mech. 842 (2018) 87–101.
[31] O.O. Fasina, Z. Colley, Viscosity and specific heat of vegetable oils as a function of temperature: 35C to 180C, Int. J. Food Prop. 11 (2008) 738–746.
[32] F. Savart, Memoire sur la constitution des veines liquides lancees par des orifices circulaires en mince paroi, Ann. Chim. 53 (1833) 337–386.
[33] Y. Tagawa, N. Oudalov, C.W. Visser, I.R. Peters, D. van der Meer, C. Sun, A. Prosperetti, D. Lohse, Highly focused supersonic microjets, Phys. Rev. X 2 (2012) 031002.
[34] S.T. Thoroddsen, K. Takehara, T.G. Etoh, C.-D. Ohl, Spray and microjets produced by focusing a laser pulse into a hemispherical drop, Phys. Fluids 21 (2009) 112101.
[35] T. Tran, H. Staat, A. Prosperetti, C. Sun, D. Lohse, Drop impact on superheated surfaces, Phys. Rev. Lett. 108 (2012) 036101.
[36] D.C.Y. Wong, M.J.H. Simmons, S.P. Decent, E.I. Parau, A.C. King, Break-up dynamics and drop size distributions created from spiralling liquid jets, Int. J. Multiphase Flow 30 (2004) 499–520.
[37] C.F. Brasz, Yang, H. Julia, C.B. Arnold, Tilting of adjacent laser-induced liquid jets, Microfluid Nanofluid 18 (2015) 185–197.